HHS Public Access

Author manuscript

J Am Chem Soc. Author manuscript; available in PMC 2017 February 27.

Published in final edited form as:

J Am Chem Soc. 2016 December 14; 138(49): 15861–15864. doi:10.1021/jacs.6b10898.

A Janus Chelator Enables Biochemically Responsive MRI Contrast with Exceptional Dynamic Range

Eric M. Gale*, **Chloe M. Jones**, **Ian Ramsay**, **Christian T. Farrar**, and **Peter Caravan**

The Athinoula A. Martinos Center for Biomedical Imaging, The Institute for Innovation in Imaging, Department of Radiology, Massachusetts General Hospital, Harvard Medical School, 149 Thirteenth Street, Suite 2301, Charlestown, Massachusetts 02129

Abstract

We introduce a new biochemically responsive Mn-based MRI contrast agent that provides a 9-fold change in relaxivity via switching between the Mn^{3+} and Mn^{2+} oxidation states. Interchange between oxidation states is promoted by a "Janus" ligand that isomerizes between binding modes that favor Mn^{3+} or Mn^{2+}. It is the only ligand that supports stable complexes of Mn^{3+} and Mn^{2+} in biological milieu. Rapid interconversion between oxidation states is mediated by peroxidase activity (oxidation) and *L*-cysteine (reduction). This Janus system provides a new paradigm for the design of biochemically responsive MRI contrast agents.

Molecular magnetic resonance imaging (MRI) adds a dimension of biochemical specificity to the rich anatomic and physiological data attainable through MRI.[1,2] Biochemical specificity is achieved either by conjugating an MRI contrast agent to a targeting vector, or engineering the contrast agent to undergo change in magnetic relaxation, or "activation," in the presence of a biochemical stimulus. Innovative chemistry has generated molecular MRI contrast agents capable of detecting protein targets,[3] pH change,[4] redox activity,[5] hypoxia,[6] ion flux,[7] neurotransmitters,[8] necrosis,[9] and enzyme activity.[10]

Sensitivity, dynamic range, and rate of response are the three main challenges to developing molecular MRI contrast agents. T_1-relaxation agents are detected at ≥10 μM (metal ion), thus only a handful of cellular and protein targets are candidates for imaging with targeted agents.[1] Activatable agents suffer from poor dynamic range. With a few notable exceptions,[3,11,12] activatable Gd-based agents rarely achieve >2-fold r_1 change in the presence of physiologically relevant levels of biochemical stimuli. Often, activatable contrast agents require prolonged incubation times before measurable relaxation change is observed.

Elegant examples of activatable agents detected via changes in the chemical exchange saturation transfer (CEST) effect have been reported,[4] but these agents are typically detected with far lower sensitivity than T_1-agents.[1]

Corresponding Author: egale@nmr.mgh.harvard.edu.

The authors declare no competing financial interests.

Supporting Information. Experimental details, synthetic procedures, compound characterization, structures not depicted in manuscript text, additional spectra, HPLC traces, and MRI acquisition parameters. The Supporting Information is available free of charge on the ACS Publications website. (PDF)

Although comparatively underexplored, coordination complexes that undergo a biochemically mediated change in paramagnetism offer a promising strategy to expand the dynamic range of activatable probes.[13–15] We, and others, have pursued biochemically activated MR contrast agents that utilize the $Mn^{3+/2+}$ couple as the activation mechanism.[16–20] The $Mn^{3+/2+}$ couple is physiologically tenable and can be tuned through ligand modifications.[21] High spin Mn^{2+} is a potent relaxation agent, whereas Mn^{3+} is a much less effective relaxation agent.[22]

Rational design of redox activated Mn-based contrast agents is challenging. Most ligand systems support a single oxidation state. Polyaminocarboxylate chelators like BPED, Chart 1, and EDTA bind Mn^{2+} with high affinity, Table S1,[23] but the redox potential of the corresponding Mn^{3+} complex is very high and the Mn^{3+} chelates decompose within seconds in aqueous media.[24] Mn^{3+} is stabilized by strongly electron releasing ligands like HBED, Chart 1, and TPPS, Fig S1. Coordination of Mn^{2+} by these ligands triggers spontaneous oxidation to Mn^{3+}.[18,25] The HBET ligand, Fig S1, stabilizes both oxidation states but the $Mn^{3+/2+}$ redox potential is >0.50 V more positive than that of tissues and cells.[26,27] Although Mn^{3+}-HBET can be prepared and is stable in aqueous solution, it does not persist in blood plasma, Figs S2–3.

We hypothesized that we could stabilize both oxidation states using a ligand that isomerizes between Mn^{3+} or Mn^{2+} selective chelators. Our prototype ligand to test this strategy, JED ("Janus HBED/BPED"), Chart 1, is designed to present a HBED-type donor set to Mn^{3+} and a BPED-type donor set to Mn^{2+}. Upon oxidation or reduction, the opposite Janus face will capture the otherwise unstable oxidation state. By analogy with previously characterized Mn^{2+} complexes with acyclic hexadentate chelators, we anticipated the Mn^{2+} complex would form a 7-coordinate, ternary complex with a rapidly exchanging water co-ligand, a requisite to high relaxivity.[28,29] The smaller Mn^{3+} ion is expected to be 6-coordinate with no inner-sphere water ligand and low relaxivity, analogous to the related $[Mn(EHPG)]^-$ complex, Fig S1.[30]

Diasteromerically pure JED (*R,R/S,S*) was isolated following a 7 step synthesis, Scheme 1. Aldol reaction of phenol and 2-pyrdinecarboxaldyde, **1**, followed by SeO_2 oxidation yielded the synthon for the Janus pyridyl-N/phenlato-O donor, **2**. Double condensation of **2** with ethylenediamine yielded **3**, which was reduced with $NaBH_4$ to a diastereomeric mixture of diamine **4**. Preparative separation of the diastereomers of **4** proved difficult, but facile separation was achieved after Zn chelation, Figs S4–5. Zn was stripped from the diastereomerically pure **4** with excess DTPA at pH 5.0. Introduction of the acetate-O donors via reductive amination of (*R,R/S,S*) **4** with glyoxylic acid yielded JED. The Mn^{2+} and Mn^{3+} complexes were independently synthesized via reaction of JED with $MnCl_2$ or MnF_3, respectively.

"BPED-type" binding of the Mn^{2+} was confirmed by UV-vis spectroscopy. Prior work with HBET and Mn^{2+}-HBET complexes showed that phenol ionization is accompanied by a significant red-shift that can be used to track phenolato-O coordination.[17] JED exhibits a similar red shift (268 to 308 nm) at pH > 10, Fig S9. The absorbance profile of Mn^{2+}-JED shows no evidence of phenol ionization out to pH 8, Fig S10. The Mn^{3+} complex can only

exist if the Janus switch to HBED-type binding occurs. HBED-type binding to Mn^{3+} is further evidenced by UV-vis spectroscopy. The Mn^{3+}-JED LMCT transitions, Fig S12, reflect those of known Mn^{3+} complexes of ligands similar to HBED.[30]

Cyclic voltammetry measurements performed on Mn-JED reveal irreversible oxidation and reduction events, Fig S11. From this data we estimate the oxidation and reduction potentials occur at 0.91 V and 0.01 V vs. NHE, respectively. The Mn-JED oxidation and reduction events mirror the Mn^{2+}-BPED oxidation event, 1.11 V, and Mn^{3+}-HBED reduction event, −0.17 V, Table S1.

The thermodynamic stability of Mn^{2+}-JED was evaluated by monitoring the direct competition reaction with BPED (log $K_{pH\ 7.4}$ = 11.2, Table S1) using HPLC (0.1 M KNO_3, RT) and yielded a log $K_{pH\ 7.4}$ = 10.8±0.2 for Mn^{2+}-JED. Mn^{2+}-JED is among the most stable Mn^{2+} complexes reported, Table S1. Direct measurement of Mn^{3+} formation constants is challenging, given the fact that the Mn^{3+} aqua ion spontaneously disproportionates to Mn^{2+} and Mn^{4+} in water. Instead, the Mn^{3+}-JED formation constant, log $K_{pH\ 7.4}$ = 28.6, was estimated from the Mn^{2+} formation constant and redox potentials,[31] Eq S3. A log $K_{pH\ 7.4}$ = 29.4 is estimated for Mn^{3+}-HBED. The congruence between the Mn^{2+}- and Mn^{3+}-JED formation constants with those of Mn^{2+}-BPED and Mn^{3+}-HBED, respectively, provides additional evidence of BPED- and HBED-type JED coordination.

The Mn^{2+} complex is a much stronger relaxation agent than its Mn^{3+} sister complex. Relaxivity values were recorded in water and human blood plasma at 1.4 T, 4.7 T and 11.7 T, 37 °C, Table 1. The Mn^{2+} vs. Mn^{3+} r_1 ratios are amongst the largest measured for any reported activatable Gd- or Mn-based relaxation agent, with a 9-fold change measured in human plasma at 1.4T. For Gd-based agents, the largest dynamic ranges reported are achieved via reactions that result in products that constrain Gd rotational dynamics.[11,12] Altering rotational dynamics provides a profound effect at field strengths ≤1.5 T, but is nearly obsolete by 3.0T.[32] Mn-JED maintains a 3.3 to 5.0-fold r_1 change at 4.7T and 11.7T. The high relaxivity of the Mn^{2+} complex is consistent with a tertiary complex with a rapidly exchanging water co-ligand. The higher relaxivity of the Mn^{2+} complex is consistent with a tertiary complex with a rapidly exchanging water co-ligand, while the lower relaxivity of the Mn^{3+} complex is consistent with a coordinatively saturated complex that precludes water coordination. The increase in relaxivity observed in blood plasma at 1.4T suggests some degree of protein binding.

Independently isolated Mn^{3+}- and Mn^{2+}-JED persist in human blood plasma at 37 °C with little inter-conversion over the course of 24 h. Mn speciation was evaluated by HPLC interfaced to an ICP for Mn detection, Fig 1. Some inter-conversion between oxidation states was observed, but the reaction proceeds slowly. Comparison of the resultant 24 h HPLC traces indicates that equilibrium had not yet been achieved. Both complexes are very stable in plasma; >95% of Mn is present as JED complexes at 24 h.

Peroxidase enzymes amplify the reactivity of reactive oxygen species. High peroxidase activity is a salient feature of the acute inflammatory response and molecular imaging of peroxidase has been pursued in animal models of vasculitis, stroke, aneurism, and

myocardial infarction.[33–36] Up to 250 U/mg (~250,000 U/mL) peroxidase activity has been measured in atherosclerotic lesions,[37] while here we show that Mn^{2+}-JED to Mn^{3+}-JED conversion is rapidly mediated by peroxidase activity 4 orders of magnitude lower than what is observed *in vivo*. Fig 2A shows HPLC traces recorded pre- and post- H_2O_2/ peroxidase incubation and confirms that conversion to Mn^{3+}-JED occurs without byproducts. Fig 2B depicts rapid peroxidase mediated oxidation of Mn^{2+}-JED, k_{obs} = 19.1±4.75 s^{-1}, in human blood plasma supplied with a steady state of H_2O_2 via the glucose/glucose oxidase reaction. Peroxidase mediated oxidation to Mn^{3+}-JED occurs on the order of seconds while in blood plasma inter-conversion between oxidation states occurs on the order of days. H_2O_2 alone triggers negligible conversion, further underscoring a selectively for peroxidase mediated oxidation. The rate measured using r_1 change tracks with the rate measured by optical absorbance at 450 nm (ε = 1180 $M^{-1}cm^{-1}$ for Mn^{3+}-JED), Figs S12–13.

Proliferating tumors are characterized by regions of hypoxia,[38] and thiol-rich microenvironments.[39,40] Mn^{3+}-JED is readily reduced to Mn^{2+}-JED in the presence of thiols. Fig 2C depicts the cysteine mediated reduction of Mn^{3+}-JED by incubation with 5 mol. equiv. *L*-Cys in blood plasma with k_{obs} = 3.60±0.50 s^{-1}. L-Cys reduction results in a remarkable 8.5-fold increase in r_1.

The MRI contrast between equimolar solutions of Mn^{2+}-JED and Mn^{3+}-JED is profound. Fig 3A shows a conventional T_1-weighted image at 4.7 T of phantoms containing 0.5 mM Mn^{2+}-JED before (−) and after (+) peroxidase mediated oxidation. In this image the higher relaxivity Mn^{2+}-JED solution is much brighter than the low relaxivity Mn^{3+}-JED solution. Gd-bis-5HT-DTPA is a state of the art peroxidase sensing Gd-based agent whose relaxivity change is mediated by a change in rotational correlation time upon oxidation, Fig S14.[41] However at 4.7 T oxidation only results in a 15% r_1 change and this small difference is highlighted in the image in Fig 3B. By using an inversion pre-pulse we can generate positive contrast in the oxidized Mn^{3+}-JED complex. Fig 3C shows the same phantoms as in 3A imaged with a 325 ms inversion pre-pulse. The inversion time was chosen to null signal in the untreated sample, generating large positive contrast in the oxidized sample. Fig 3D shows the same inversion pre-pulse sequence applied to the Gd-bis-5HT-DTPA samples from Fig 3B. Regardless of the scanning protocol, the contrast generated following oxidation of the Mn-based agent is much larger than that possible with the Gd-based agent. Fig 3E compares percentage r_1 change observed afer peroxidase oxidation of Mn-JED and Gd-bis-5HT-DTPA at 4.7 T. The Mn agent undergoes 380% r_1 change whereas the activatable Gd-based agents experiences <15% r_1 change. At 1.4 T, the r_1 change is also much greater for the Mn-JED system (790%) than for Gd-bis-5HT-DTPA (60%). Images of phantoms prepared in human blood plasma exhibit comparable contrast, Fig S15.

To our knowledge, JED is the only chelator capable of stabilizing both Mn^{3+} and Mn^{2+} in the physiological milieu, and enables rapid and reversible biochemically mediated interconversion between Mn^{3+} (low r_1) and Mn^{2+} (high r_1). The biochemically mediated r_1 change observed with Mn-JED is the largest of any activatable Gd- or Mn-based contrast agent. Peroxidase mediated oxidation of Mn^{2+}- to Mn^{3+}-JED provides over an order of magnitude greater r_1 change than the state of the art Gd-based peroxidase sensor, and is

achieved in minutes at peroxidase concentrations 1000-fold below what is seen *in vivo*. Mn-JED offers a promising new paradigm for activatable MRI contrast agent development.

Supplementary Material

Refer to Web version on PubMed Central for supplementary material.

Acknowledgments

This work was supported by grants from the National Heart, Lung, and Blood Institute (K25HL128899), the National Institute of Biomedical Imaging and Bioengineering (R01EB009062, R21EB022804) and instrumentation funded by the National Center for Research Resources and the Office of the Director (P41RR14075, S10RR023385, S10OD010650).

References

1. Boros E, Gale EM, Caravan P. Dalton Trans. 2015; 44:4804. [PubMed: 25376893]
2. Angelovski G. Angew Chem Int Ed. 2016; 55:7038.
3. Caravan P. Acc Chem Res. 2009; 42:851. [PubMed: 19222207]
4. De Leon-Rodriguez LM, Lubag AJM, Malloy CR, Martinez GV, Gillies RJ, Sherry AD. Acc Chem Res. 2009; 42:948. [PubMed: 19265438]
5. Tsitovich PB, Burns PJ, McKay AM, Morrow JR. J Inorg Biochem. 2014; 133:143. [PubMed: 24529651]
6. Do QN, Ratnakar SJ, Kovács Z, Sherry AD. ChemMedChem. 2014; 9:1116. [PubMed: 24825674]
7. Lubag AJM, De León-Rodríguez LM, Burgess SC, Sherry AD. Proc Natl Acad Sci, USA. 2011; 108:18400. [PubMed: 22025712]
8. Lee TY, Cai LX, Lelyveld VS, Hai A, Jasanoff A. Science. 2014; 344:533. [PubMed: 24786083]
9. Huang S, Chen HH, Yuan H, Dai G, Schühle DT, Mekkaoui C, Ngoy S, Liao R, Caravan P, Josephson L, Sosnovik DE. Circ Cardiovasc Imaging. 2011; 4:729. [PubMed: 21836081]
10. Hingorani DV, Bernstein AS, Pagel MD. Contrast Media Mol Imaging. 2014; 10:245. [PubMed: 25355685]
11. Yu J, Martins AF, Preihs C, Jordan VC, Chirayil S, Zhao P, Wu Y, Nasr K, Kiefer GE, Sherry AD. J Am Chem Soc. 2015; 137:14173. [PubMed: 26462412]
12. Nivorozhkin AL, Kolodziej AF, Caravan P, Greenfield MT, Lauffer RB, McMurry TJ. Angew Chem Int Ed. 2001; 40:2903.
13. Ekanger LA, Ali MM, Allen MJ. Chem Commun. 2014; 50:14835.
14. Ekanger LA, Polin LA, Shen Y, Haacke EM, Martin PD, Allen MJ. Angew Chem Int Ed. 2015; 54:14398.
15. Tsitovich PB, Spernyak JA, Morrow JR. Angew Chem Int Ed. 2013; 52:13997.
16. Loving GS, Mukherjee S, Caravan P. J Am Chem Soc. 2013; 135:4623.
17. Gale EM, Mukherjee S, Liu C, Loving GS, Caravan P. Inorg Chem. 2014; 53:10748. [PubMed: 25226090]
18. Aime S, Botta M, Gianolio E, Terreno E. Angew Chem Int Ed. 2000; 39:747.
19. Yu M, Ambrose SL, Whaley ZL, Fan S, Gorden JD, Beyers RJ, Schwartz DD, Goldsmith CR. J Am Chem Soc. 2014; 136:12836. [PubMed: 25187295]
20. Yu M, Beyers RJ, Gorden JD, Cross JN, Goldsmith CR. Inorg Chem. 2012; 51:9153. [PubMed: 22889331]
21. Jackson TA, Karapetian A, Miller AF, Brunold TC. J Am Chem Soc. 2004; 126:12477. [PubMed: 15453782]
22. Lauffer RB. Chem Rev. 1987; 87:901.
23. Lacoste RG, Christoffers GV, Martell AE. J Am Chem Soc. 1965; 87:2385.
24. Hamm RE, Suwyn MA. Inorg Chem. 1967; 6:139.

25. Frost AE, Freedman HH, Westerback SJ, Martell AE. J Am Chem Soc. 1958; 80:530.
26. Jones DP, Carlson JL, Mody VC Jr, Cai J, Lynn MJ, Sternberg P Jr. Free Rad Biol Med. 2000; 28:625. [PubMed: 10719244]
27. Kirlin WG, Cai J, Thompson SA, Diaz D, Kavanagh TJ, Jones DP. Free Rad Biol Med. 1999; 27:1208. [PubMed: 10641713]
28. Drahoš B, Lukeš I, Tóth E. Eur J Inorg Chem. 2012; 2012:1975.
29. Gale EM, Atanasova I, Blasi F, Ay I, Caravan P. J Am Chem Soc. 2015; 137:15548. [PubMed: 26588204]
30. Bihari S, Smith PA, Parsons S, Sadler PJ. Inorg Chim Acta. 2001; 331:310.
31. Rorabacher DB. Chem Rev. 2004; 104:651. [PubMed: 14871138]
32. Caravan P, Farrar CT, Frullano L, Uppal R. Contrast Media Mol Imag. 2009:89.
33. Su HS, Nahrendorf M, Panizzi P, Breckwoldt MO, Rodriguez E, Iwamoto Y, Aikawa E, Weissleder R, Chen JW. Radiology. 2012; 262:181. [PubMed: 22084204]
34. Nahrendorf M, Sosnovik D, Chen JW, Panizzi P, Figueiredo JL, Aikawa E, Libby P, Swirski FK, Weissleder R. Circulation. 2008; 117:1153. [PubMed: 18268141]
35. Breckwoldt MO, Chen JW, Stangenberg L, Aikawa E, Rodriguez E, Qiu S, Moskowitz MA, Weissleder R. Proc Natl Acad Sci, USA. 2008; 105:18584. [PubMed: 19011099]
36. DeLeo MJ III, Gounis MJ, Hong B, Ford JC, Wakhloo AK, Bogdanov AA Jr. Radiology. 2009; 252:696. [PubMed: 19546428]
37. Daugherty A, Dunn JL, Rateri DL, Heinecke JW. J Clin Invest. 1994; 94:437. [PubMed: 8040285]
38. Bourgeois M, Rajerison H, Guerard F, Mougin-Degraef M, Barbet J, Michel N, Cherel M, Faivre-Chauvet A, Gestin JF. Nucl Med Rev. 2011; 14:90.
39. Kuppusamy P, Li H, Ilangovan G, Cardounel AJ, Zweier JL, Yamada K, Krishna MC, Mitchell JB. Cancer Res. 2002; 62:307. [PubMed: 11782393]
40. Jorgenson TC, Zhong W, Oberley TD. Cancer Res. 2013; 73:6118. [PubMed: 23878188]
41. Rodríguez E, Nilges M, Weissleder R, Chen JW. J Am Chem Soc. 2010; 132:168. [PubMed: 19968300]

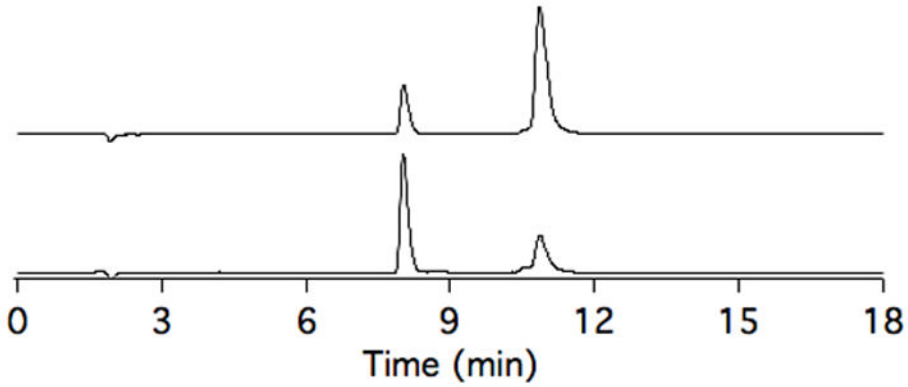

Figure 1.

HPLC-ICP-MS traces showing Mn speciation of solutions of Mn^{2+}-JED (top trace) and Mn^{3+}-JED (bottom trace) incubated for 24 h, 37 °C, in human blood plasma. Mn^{3+}- and Mn^{2+}-JED elute at 8.0 and 10.9 min. Inter-conversion between the Mn^{3+}- and Mn^{2+}-complexes is slow, not reaching equilibrium within 24h.

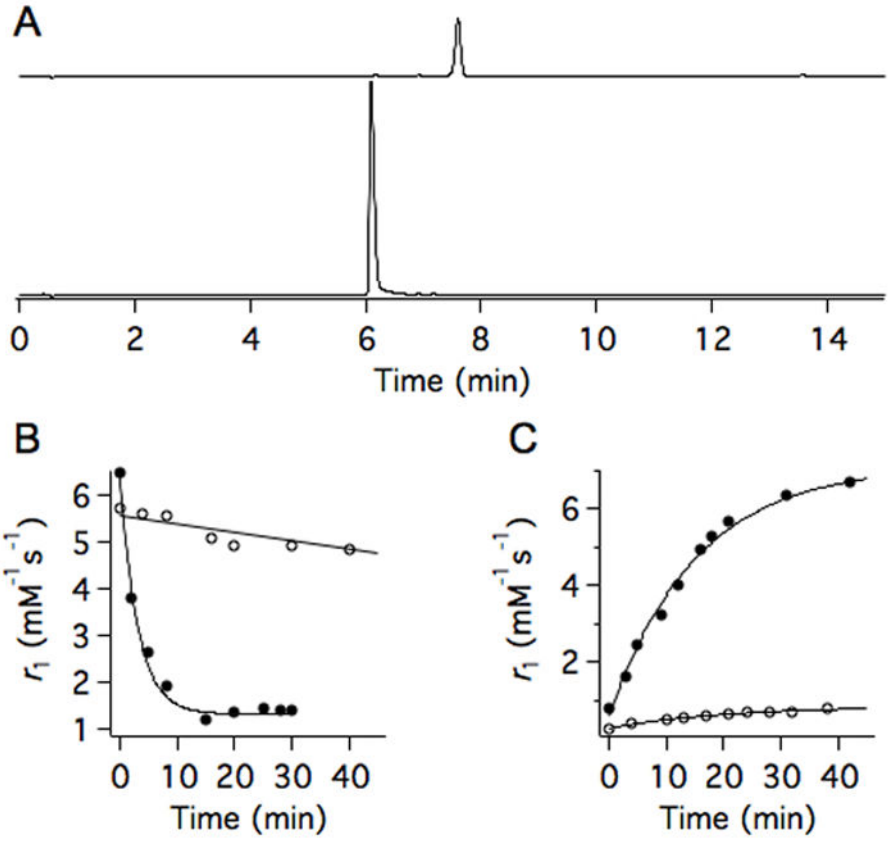

Figure 2.

Biochemically mediated interconversion of Mn-JED oxidation states by peroxidase and thiols. (A) Conversion of Mn^{2+}-JED (top trace, 7.6 min) to Mn^{3+}-JED (bottom trace, 6.1 min) triggered by H_2O_2/ peroxidase (25 U/mL) in PBS buffer monitored by HPLC with 254 nm detection. The difference in peak height between the pre- and post-peroxidase treated samples results from the 2-fold higher extinction co-efficient of Mn^{3+}-JED. (B) Oxidation of Mn^{2+}-JED in the presence of H_2O_2 (open circles) or H_2O_2/peroxidase (15 U/mL, closed circles) in human blood plasma monitored by NMR. H_2O_2 was generated in situ by the glucose/ glucose oxidase reaction. (C) Reduction of Mn^{3+}-JED in human blood plasma without (open circles) and with 5 mol. equiv. *L*-Cys (filled circles) added. Relaxometry measurements were performed at 1.4T, 37 °C.

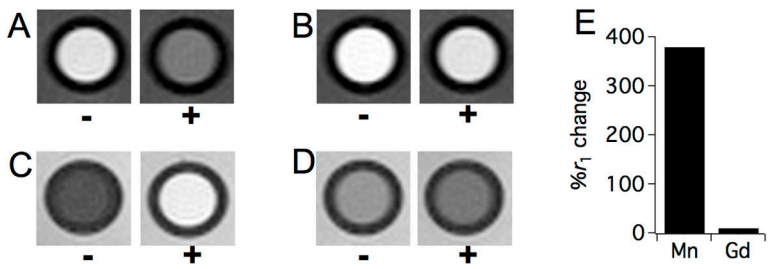

Figure 3.

MR phantom images at 4.7 T, RT, of water with 0.5 mM Mn^{2+}-JED (A and C) or Gd-bis-5HT-DTPA (B and D) before (−) and after (+) incubation with H_2O_2/ peroxidase (45 U/mL). Images (A and C) acquired using a T_1-weighted FLASH sequence, or (B and D) with a 325 ms inversion pre-pulse to generate large positive contrast in the oxidized sample; see SI for image acquisition details. Note the high contrast between the samples containing Mn^{2+}- vs. Mn^{3+}-JED, but low contrast for the Gd-based system. (E) Percentage r_1 change after peroxidase mediated oxidation of the Mn- and Gd- based agents. A detailed description of the scanning parameters is in the SI.

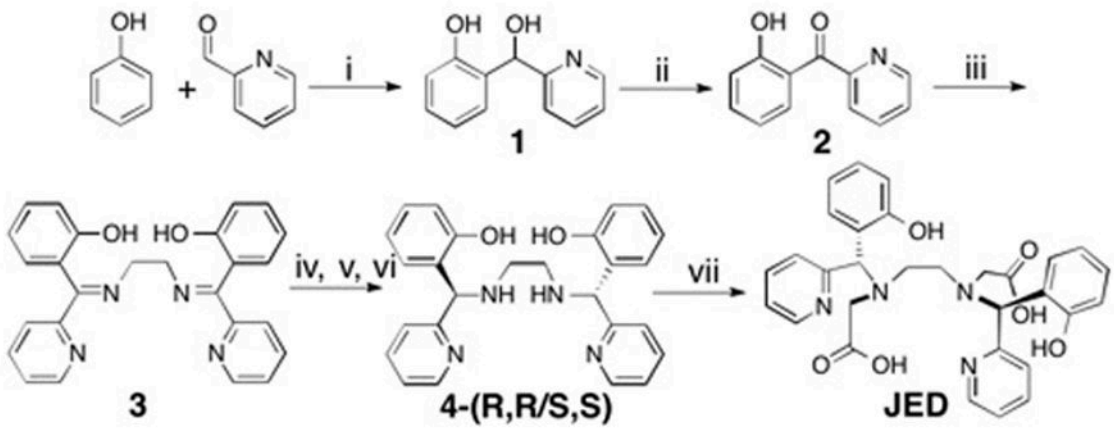

Scheme 1. Synthesis of JED[a,b]

[a](i) $MgCl_2$, Me_2NEt, CH_2Cl_2, RT; (ii) SeO_2, dioxane, 100 °C; (iii) 0.5 mol. equiv. ethylenediamine, MeOH, RT; (iv) $NaBH_4$, (v) $Zn(OTf)_2$, 1:1 MeCN:H_2O, RT – diastereomers of Zn•**4** separated by RP-HPLC; (vi) excess DTPA, pH 5.0; (vii) glyoxylic acid, $NaBH_3CN$, $NaHCO_3$, MeOH. [b]JED was prepared from the (*R,R/S,S*) diastereomer of **4**; (*S,S*) **4** and JED are depicted here.

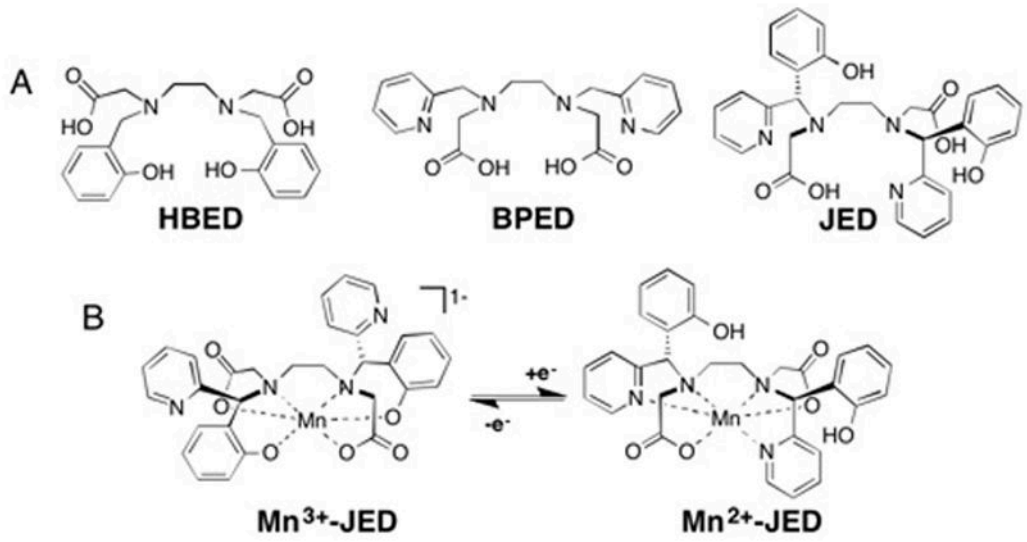

Chart 1.

(A) Mn^{3+} and Mn^{2+} selective chelators, HBED and BPED, respectively, and the Janus chelate, JED, designed to support both Mn^{3+}- and Mn^{2+}. (B) Redox triggered isomerization of Mn^{3+}- and Mn^{2+}-JED.

Table 1

Relaxivity values, r_1, of Mn^{3+}- and Mn^{2+}-JED recorded in water or human plasma (in parenthesis) at 1.41T, 4.7T[a] or 11.7T, 37 °C. Relaxivity of Mn^{2+}-JED is much higher regardless of applied field strength.

	Mn^{3+}	Mn^{2+}	r_1 Mn^{2+}/ r_1 Mn^{3+}
1.4T	0.5±0.01 (0.9±0.01)	3.3±0.06 (8.0±0.39)	6.6 (8.9)
4.7T[a]	0.9±0.02 (1.1±0.05)	4.3±0.32 (3.6±0.21)	4.8 (3.3)
11.7T	0.5±0.01 (0.5±0.02)	2.5±0.08 (1.9±0.08)	5.0 (4.8)

[a]4.7T measurements performed at RT.

J Am Chem Soc. Author manuscript; available in PMC 2017 February 27.